A Molecular Communication Perspective on Detecting Arterial Plaque Formation

Pit Hofmann*, *Graduate Student Member, IEEE*, Sebastian Schmidt*, *Graduate Student Member, IEEE*, Alexander Wietfeld*, *Graduate Student Member, IEEE*, Pengjie Zhou, Jonas Fuchtmann, Frank H.P. Fitzek, *Senior Member, IEEE*, and Wolfgang Kellerer, *Senior Member, IEEE*

***Abstract*—The formation of plaques in human blood vessels, known as *atherosclerosis*, represents one of the major causes of death worldwide. Molecular communication (MC) in combination with nanotechnology is envisioned to enable novel approaches towards diagnosing, monitoring, and treating diseases. In this paper, we propose an investigation of the effects of plaque formation on the human blood vessel as an MC channel. By characterizing these changes, the early detection of plaques using MC networks in the human circulatory system could become possible. Using OpenFOAM, we model a simplified blood flow scenario in a human carotid artery. Nanoparticles are released in the bloodstream in front of a region obstructed by a plaque, and their transport and distribution are evaluated as they pass through. The results are obtained for different plaque sizes and channel lengths. We observe a significant impact of a growing plaque on the channel characteristics in terms of a reduced propagation delay and a decrease in the cumulative number of received particles due to particles trapped by the plaque. Therefore, the receiver could detect abnormal conditions from a change in these channel conditions over time. Further investigation of these methods in conjunction with more realistic modeling of the channel and communication nodes will be necessary to confirm the results and could contribute towards advanced future methods of diagnosis.**

***Index Terms*—Internet of Bio-Nano Things, microfluidic molecular communication, OpenFOAM, plaque formations, simulation**

I. Introduction

THE convergence of nanotechnology and communication paradigms has paved the way for innovations in the field of bioengineering and healthcare. Among these innovations, molecular communication (MC) stands out as a promising paradigm for enabling communication at the nanoscale, facilitating the exchange of information among bio-nano machines (BNM) [1]. The emerging concept of the Internet of Bio-Nano Things (IoBNT) has gained attention, providing a networked ecosystem where BNM communicate to monitor and control various biological processes [1]. One intriguing application of the IoBNT could lie in addressing the issue of arterial plaque formation or *atherosclerosis*. This paper explores the interdisciplinary synergy in MC between biology, nanotechnology, and communications engineering, and their potential role in early plaque detection strategies to address this pervasive health challenge.

In the envisioned scenario, a large number of BNM is deployed within the human cardiovascular system. The BNM communicate using nanoparticles or molecules which are transported by diffusion and flow through the blood vessels. These BNM serve as agents for combating plaque formations through various mechanisms. Firstly, they can release specific molecules or drugs from onboard reservoirs into the bloodstream to counteract critical plaque formations, offering a localized therapeutic response, i.e., targeted drug delivery [2]. Secondly, the BNM can use MC, orchestrating the release of messenger substances or endogenous hormones from the body's own resources to aid in plaque control within non-critical areas.

In this paper, we focus on combining ongoing MC research with the concept of sensing and detecting health risks in the form of plaque formation using the example of the carotid artery. Therefore, we model the blood flow in a blood vessel using OpenFOAM, adding plaque of varying sizes (i.e., at different stages of growth). From an analytical point of view, we need accurate MC channel models for the design, analysis, and reliable operation of MC systems [3]. The state-of-the-art [3] channel models for advection do not yet consider obstacles, e.g., plaque formations, in the communication channel. In [4], a number of different obstacles were placed in an experimental system and were found to not degrade or even improve communication performance. However, the investigated system was of a much larger scale than blood vessels. In [5], shapes were examined via simulations, specifically as decelerators in the flow channel, to reduce the dispersion of the MC pulse. The scale used is similar to blood vessels, and the obstacles are found to have both accelerating and decelerating effects. But, in this case, obstacles were deliberately designed to benefit the communication. In none of the papers the obstacles were interpreted as a medical sensing issue. In contrast, we propose to use an undesirable and initially unknown change in channel conditions due to the narrowing channel and the change in flow speed in the region of the plaque as an indicator for

Alexander Wietfeld, Sebastian Schmidt, and Wolfgang Kellerer are with the Chair of Communication Networks, Technical University of Munich, Germany, email: {alexander.wietfeld, sebastian.a.schmidt, wolfgang.kellerer}@tum.de.

Pit Hofmann, Pengjie Zhou, and Frank H.P. Fitzek are with the Deutsche Telekom Chair of Communication Networks, Technische Universität Dresden, Dresden, Germany; F. Fitzek is also with the Centre for Tactile Internet with Human-in-the-Loop (CeTI), Dresden, Germany, email: {pit.hofmann, pengjie.zhou, frank.fitzek}@tu-dresden.de.

Jonas Fuchtmann is with the Minimally Invasive Interdisciplinary Therapeutical Intervention (MITI), Klinikum rechts der Isar, Technical University Munich, Munich, Germany, email: jonas.fuchtmann@tum.de.

This work was supported by the German Research Foundation (DFG) as part of Germany's Excellence Strategy—EXC 2050/1—Cluster of Excellence "Centre for Tactile Internet with Human-in-the-Loop" (CeTI) of Technische Universität Dresden under project ID 390696704 and the Federal Ministry of Education and Research (BMBF) in the programme of "Souverän. Digital. Vernetzt." Joint project 6G-life, grant number 16KISK001K and 16KISK002.

*P. Hofmann, S. Schmidt, and A. Wietfeld contributed equally to this work and are listed as co-first authors in alphabetical order of the surnames.

the detection of the plaque itself. This could be implemented via dedicated periodic pilot symbols sent by the BNM in the bloodstream or alternatively by interpreting the received signal from symbols sent for the purpose of unrelated MC between the BNM, for example, synchronization messages, resulting in a type of joint communication and sensing scheme.

II. Medical Implications of Plaque Formation

The formation of plaque within human arteries, a process known as *atherosclerosis* [6], is a complex and multifaceted phenomenon with significant implications for human cardiovascular health. *Atherosclerosis* involves the gradual accumulation of lipids, inflammatory cells, and fibrous tissue within the arterial walls, leading to the development of *atherosclerotic* plaques. These plaques can compromise the blood flow, increasing the risk of ischemic events like strokes. Several risk factors contribute to the development of a plaque, including hypertension, hyperlipidemia, smoking, and diabetes. Therefore, *atherosclerosis* represents a significant health problem, being the most common cause of cardiac death and constituting about 30 % of all deaths worldwide [7].

Specifically, plaques in the carotid artery are estimated to affect about 21.1 % of the world's population between the ages of 30 and 79, with an increase in the elderly demographic [8]. Recent advances in the treatment of carotid artery disease include interventions like carotid endarterectomy and carotid artery stenting, aiming to restore adequate blood flow and reduce the risk of adverse cardiovascular events. Therefore, measures to react to carotid artery plaques are available, while at the same time, early-stage preventive diagnosis is not yet standard practice. Leveraging continuous communication inside the body as part of a future IoBNT could be a path towards monitoring and early detection of diseases, e.g., carotid artery plaque.

III. Microfluidic MC Simulation

A. Model Setup

In our three-dimensional (3D) scenario, we address the plaque formation in human carotids. The model follows Fig. 1. We assume a circular uniform transmitter and a circular observing receiver. The distance l_c between transmitter and receiver, i.e., the length of the channel, is constant. We assume a constant distance of $l_c \in \{50, 100\}$ mm. For the radius of the channel modeling the human carotid, r_c, we assume $r_c = 3.0\,\mathrm{mm}$ (diameter d_c is equal to $6.0\,\mathrm{mm}$ [9]). Furthermore, we assume a constant *Poiseuille* flow with a mean velocity $v_{\mathrm{eff}} = 34.2\,\mathrm{cm/s}$, which is a good estimate for the blood flow velocity in common human carotid arteries [9]. Modeling the plaque formation, r_p denotes the reduction in artery radius due to the plaque. In the following, we refer to r_p relative to r_c. On the one hand, we consider the default case, which means that $r_p = 0 \times r_c$, i.e., the channel is a tube without any plaque formation. In addition, we consider the cases $r_p = 0.25 \times r_c$, $r_p = 0.5 \times r_c$, and $r_p = 0.75 \times r_c$. $l_{\mathrm{p,inner}}$ and $l_{\mathrm{p,outer}}$ denote the length of the plaque at the outside of the blood vessel and the length of the plaque inside the blood vessel, respectively. $l_{\mathrm{p,inner}} = 10.0\,\mathrm{mm}$ and $l_{\mathrm{p,outer}} = 20.0\,\mathrm{mm}$ are assumed to be constant. An overview of all simulation parameters can be found in Table I.

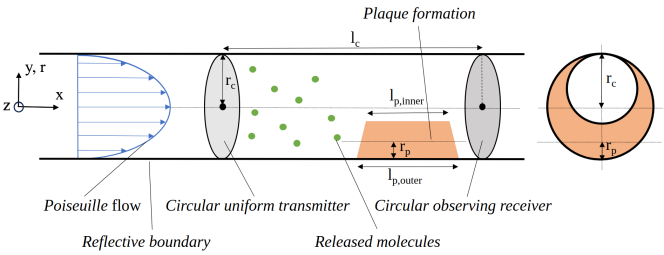

Fig. 1. Channel model for the considered plaque scenario.The figure on the left shows the longitudinal section of the model, the figure on the right the cross-section.

TABLE I
Simulation Parameters

Parameter	Value
Channel length l_c [mm]	$\{50, 100\}$
Radius r_c [mm]	3.0
Mean velocity v_{eff} [cm/s]	34.2
Radial expansion plaque r_p	$\{0, 0.25, 0.5, 0.75\} \times r_c$
Length plaque inside $l_{p,\mathrm{inner}}$ [mm]	10
Length plaque outside $l_{p,\mathrm{outer}}$ [mm]	20

B. Fluid, Particle, and Wall Parameters

1) Fluid Properties: Targeting future use case families in the IoBNT, we consider human blood as a fluid for our simulations. We assume a blood density of $1050\,\mathrm{kg/m^3}$ [10]. The fluid properties in OpenFOAM, analogous to [11], are based on the non-Newtonian *Bird-Carreau* model of blood [12]. The blood's kinetic viscosity ν changes with respect to the fluid's rate of shear stress $\dot{\gamma}$ as

$$\nu = \nu_\infty + (\nu_0 - \nu_\infty)[1 + (k\dot{\gamma})^a]^{\frac{n-1}{a}}, \tag{1}$$

where ν_0, ν_∞, k, and n denote the kinematic viscosity of the fluid at zero shear rate, the kinematic viscosity of the fluid at infinite shear rate, the relaxation time, and the power index, respectively. a is a variable that takes into account the change from linear behavior to power law. We assume the following parameters [11]: $\nu_0 = 3.3 \times 10^{-6}\,\mathrm{m^2/s}$, $\nu_\infty = 1.32 \times 10^{-5}\,\mathrm{m^2/s}$, $k = 0.6046\,\mathrm{s}$, $n = 0.3742$, and $a = 2$.

2) Particle Properties: We assume superparamagnetic iron-oxide nanoparticles (SPIONs) as information carriers. SPIONs comprise an iron core accompanied by a biocompatible lauric acid coating to prevent clumping, typically possessing a hydrodynamic radius of 50 nm [13]. Due to their biocompatibility, SPIONs have found applications in various medical contexts, e.g., in targeted drug delivery [14]. For the simulation study, we assume a fixed value size distribution. A total number of $n = 1000$ nanoparticles is released after reaching the quasi-stationary state. Following Fig. 2, the quasi-stationary state is achieved after approximately 0.3 s for both values of l_c. The start of injection (SOI), i.e., the release of the SPIONs, is defined as 0.4 s. The nanoparticles are released uniformly distributed over the entire cross-section of the circular uniform transmitter. We assume a density of $5175\,\mathrm{kg/m^3}$ [15].

TABLE II
BOUNDARY CONDITIONS FOR THE VELOCITY AND THE PRESSURE.

Boundary	**Patch**	**Type**	**Value**
Velocity [m/s]	inlet	*fixedValue*	$[0.342, 0, 0]$
	outlet	*inletOutlet*	$[0, 0, 0]$
	walls	*noSlip*	–
Kinematic pressure $[m^2/s^2]$	inlet	*fixedFluxPressure*	uniform 0
	outlet	*fixedValue*	uniform 0
	walls	*fixedFluxPressure*	uniform 0

3) Wall Properties: Analogous to [11], the walls are modeled as a rigid surface. Thereby, on the vessel wall, *noSlip* boundary conditions are applied. The *noSlip* boundary condition sets the patch velocity in all three spatial directions to zero, i.e., $\mathbf{v_{wall}} = [0\ 0\ 0]$.

C. Boundary Conditions

At the inlet, the boundary condition for the velocity is specified as *fixedValue*. Consequently, the velocity at the inlet face is defined by the vector $[0.342\ 0\ 0]$ m/s across all three spatial directions, assuming a fluid flow velocity of $v_{\text{eff}} = 34.2\,\text{cm/s}$. For the walls, the boundary condition *noSlip* is applied, enforcing zero velocity at the patch in all three spatial directions. At the outlet, the *inletOutlet* boundary condition establishes the outflow of the system by imposing a zero gradient condition. This condition ensures that the field adopts the internal field value, maintaining continuity in the absence of a significant gradient at the outlet.

The pressure boundary condition at the inlet and at the walls is applied by the *fixedFluxPressure* condition. The *fixedFluxPressure* condition is employed in pressure scenarios, commonly incorporating the zero gradient condition. Conversely, the *fixedValue* condition is applied at the outlet. Table II provides an overview of the boundary conditions.

D. Fluid Flow Parameters

All simulation cases are simulated assuming laminar flow — in this first measurement study, we neglect turbulence modeling. One can differentiate between laminar and turbulent flows by considering the ratio of the inertial forces to the viscous forces, known as the *Reynolds* number. The *Reynolds* number for flow in a pipe can be computed as [16]:

$$Re = \frac{v_{\text{eff}} \cdot D_H}{\nu}, \tag{2}$$

whereby v_{eff}, D_H, and ν denote the mean velocity in the tube, the hydraulic diameter of the tube (for a circular tube the hydraulic diameter is equal to the diameter of the tube), and the kinematic viscosity. For $v_{\text{eff}} = 0.342\,\text{m/s}$, $D_H = 0.006\,\text{m}$, and $\nu = \{\nu_0, \nu_\infty\} = \{3.3 \times 10^{-6}, 1.32 \times 10^{-5}\}\text{m}^2/\text{s}$, it follows for the plain tube: $Re = \{621.82, 155.45\} < 2300$ [16], i.e., laminar flow regime. This is only a preliminary estimation for this initial study as turbulence modeling for non-Newtonian fluids and in a pipe with changing diameter is beyond the scope of this paper.

In our simulation runs, we simulate a total time of 1.4 s, i.e., SOI plus 1 s simulation time of the released particles. The time interval Δt for the simulation runs is constant, $\Delta t = 1 \times 10^{-4}\,\text{s}$.

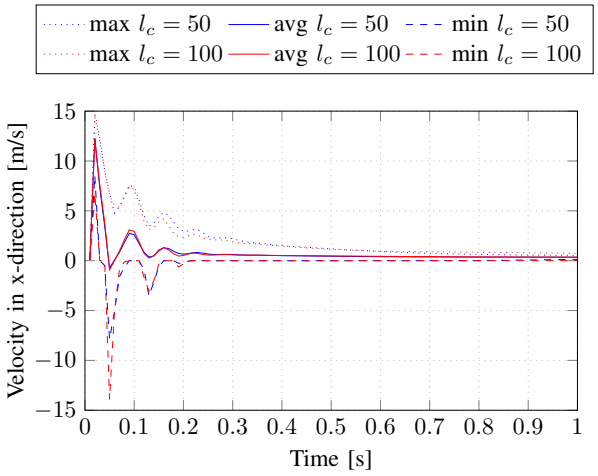

Fig. 2. Convergence to a steady state for various distances l_c (in mm) conducted using the *simpleFoam* solver, excluding any interaction with injected particles. A quasi-stationary state is achieved in the two scenarios after approximately 0.3 s.

IV. RESULTS AND DISCUSSION

Fig. 3 shows the channel impulse response (CIR), i.e., the fraction of the received molecules, for both transmitter-receiver distances, namely $l_c = 50\,\text{mm}$ and $l_c = 100\,\text{mm}$. In both scenarios, we see that the larger the radius of the plaque r_p, i.e., the smaller the narrowed cross-section of the channel, the sooner the released molecules reach the receiver. For example, for $l_c = 100\,\text{mm}$, the first molecules arrive at the receiver 0.58 s after the SOI for the plain tube ($r_p = 0$), while for $r_p = 0.25 \times r_c$, $r_p = 0.5 \times r_c$, and $r_p = 0.75 \times r_c$ the first molecules arrive 0.56 s, 0.54 s, and 0.52 s after the SOI, respectively. The faster arrival of the particles can be explained by the higher flow velocity in the narrowed channel caused by the Venturi effect [17]. Furthermore, it can be seen that the height of the peak increases up to $r_p = 0.5 \times r_c$, followed by a decrease which, however, decreases with increasing distance between transmitter and receiver. An increase in channel length from 50 mm to 100 mm is associated with an added propagation delay of about 0.1 s and an increase in particle dispersion over time.

Fig. 4 depicts the cumulative CIR, i.e., the total number of received molecules over time for the different values of r_p and l_c. Analogous to Fig. 3, the faster arrival of the molecules for larger plaques is represented by the earlier rise in the number of molecules. Except for an added propagation delay, the channel length does not seem to impact the results significantly. Fig. 4 also depicts the asymptotic number of received molecules, which appears to have reached a stable plateau in all cases at the end of the simulation. As expected, the plateau is reached faster for larger plaque sizes. Additionally and crucially, we also see a decrease in the asymptotic number of received molecules for a growing plaque, i.e., some molecules do not arrive at the receiver. While for $r_p \in \{0, 0.25\} \times r_c$, this fraction remains at 0%, for $r_p = 0.5 \times r_c$, approximately 5%, and for $r_p = 0.75 \times r_c$, around 25% of molecules do not reach the receiver. An analysis of the 3D flow simulation results reveals that the plaque prevents some molecules from moving on to

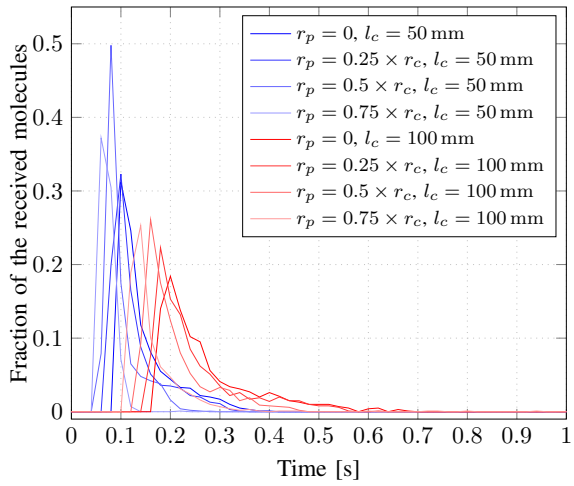

Fig. 3. Fraction of the received molecules compared to the $n = 1000$ released molecules for the two transmitter-receiver distances $l_c = 50\,\text{mm}$, and $l_c = 100\,\text{mm}$.

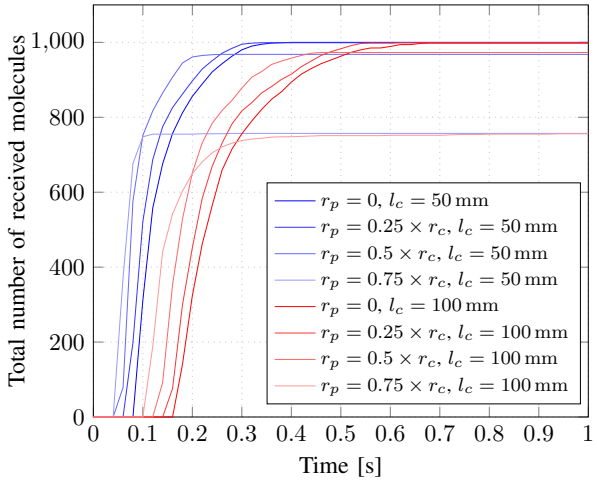

Fig. 4. Total number of the received molecules for the two transmitter-receiver distances $l_c = 50\,\text{mm}$, and $l_c = 100\,\text{mm}$.

the receiver, resulting in them not arriving or only arriving very slowly.

This effect on the asymptotic number of molecules could be a crucial indicator of a growing plaque, as it is a marker which appears in the long-term consideration of the channel response and does not require precise timing or peak detection. It also explains the lowering of the peak for plaque radii greater than $0.5 \times r_c$ observed in Fig. 3 since the decrease in the total number of contributing molecules will naturally also decrease the peak number of molecules that pass through over time.

V. Conclusion and Future Research

In this paper, we have evaluated the effect of arterial plaque of different sizes on the CIR for a simplified MC link within a blood vessel. The results show that growing plaque is associated with a lower propagation delay and a reduction in the total number of received molecules, as plaques with a radius $> 0.25 \times r_c$ prevent some nanoparticles from passing through the channel. It is important to note that this result, in particular, is dependent on our assumptions on the surface roughness resulting in stoppage of the particles, and a further investigation of more detailed models of arteries as MC channels is crucial for future work. However, increased surface roughness has previously been identified as a feature of sites of plaque growth, and they could, therefore, be associated with a higher likelihood of inhibiting some particles [18].

This is a preliminary step towards analyzing cardiovascular diseases from the perspective of communication theory in the context of the IoBNT vision, where BNM communicate inside the body. Future research will include more detailed arterial properties and more complex plaque formation scenarios. Investigating the complex effects of turbulence on the propagation will also be an essential next step to capture more detailed results.

References

[1] I. F. Akyildiz, M. Pierobon, S. Balasubramaniam, and Y. Koucheryavy, "The Internet of Bio-Nano Things," *IEEE Commun. Mag.*, vol. 53, no. 3, Mar. 2015.

[2] U. A. K. Chude-Okonkwo, R. Malekian, B. T. Maharaj, and A. V. Vasilakos, "Molecular communication and nanonetwork for targeted drug delivery: A survey," *IEEE Commun. Surv. Tutor.*, vol. 19, no. 4, May 2017.

[3] V. Jamali, A. Ahmadzadeh, W. Wicke, A. Noel, and R. Schober, "Channel modeling for diffusive molecular communication—A tutorial review," *Proc. IEEE*, vol. 107, no. 7, Jun. 2019.

[4] I. Atthanayake, S. Esfahani, P. Denissenko, I. Guymer, P. J. Thomas, and W. Guo, "Experimental Molecular Communications in Obstacle Rich Fluids," in *Proc. 5th ACM Int. Conf. Nanoscale Comput. Commun.*, short paper, Reykjavik Iceland, Sep. 2018.

[5] A. S. Thalmayer, A. Ladebeck, S. Zeising, and G. Fischer, "Reducing Dispersion in Molecular Communications by Placing Decelerators in the Propagation Channel," *IEEE Trans. Mol. Biol. Multi-Scale Commun.*, Jul. 2023.

[6] R. Ross, "Atherosclerosis — An inflammatory disease," *New England Journal of Medicine*, vol. 340, no. 2, Jan. 1999.

[7] V. R. Preedy and R. R. Watson, Eds., *Handbook of Disease Burdens and Quality of Life Measures*. New York, NY: Springer, 2010.

[8] P. Song, Z. Fang, H. Wang, et al., "Global and regional prevalence, burden, and risk factors for carotid atherosclerosis: a systematic review, meta-analysis, and modelling study," *The Lancet Global Health*, vol. 8, no. 5, May 2020.

[9] L. A. Ferrara, M. Mancini, R. Iannuzzi, et al., "Carotid diameter and blood flow velocities in cerebral circulation in hypertensive patients," *Stroke*, vol. 26, no. 3, Mar. 1995.

[10] T. Kenner, "The measurement of blood density and its meaning," *Basic Research in Cardiology*, vol. 84, no. 2, Mar. 1989.

[11] S. Yogeswaran and F. Liu, "Vascular flow simulations using SimVascular and OpenFOAM," *medRxiv*, Sep. 2021.

[12] Y. I. Cho and K. R. Kensey, "Effects of the non-Newtonian viscosity of blood on flows in a diseased arterial vessel. Part 1: Steady flows," *Biorheology*, vol. 28, no. 3-4, Jun. 1991.

[13] M. Bartunik, J. Teller, G. Fischer, and J. Kirchner, "Channel parameter studies of a molecular communication testbed with biocompatible information carriers: Methods and data," *IEEE Trans. Mol. Biol. Multi-Scale Commun.*, vol. 9, no. 4, Oct. 2023.

[14] R. Tietze, S. Lyer, S. Dürr, et al., "Efficient drug-delivery using magnetic nanoparticles — Biodistribution and therapeutic effects in tumour bearing rabbits," *Nanomedicine: NBM*, vol. 9, no. 7, Oct. 2013.

[15] M. Kappes, B. Friedrich, F. Pfister, et al., "Superparamagnetic iron oxide nanoparticles for targeted cell seeding: Magnetic patterning and magnetic 3D cell culture," *Adv. Funct. Mater.*, vol. 32, no. 50, Aug. 2022.

[16] F. White, *Fluid mechanics* (McGraw-Hill International Editions). WCB/McGraw-Hill, 1999.

[17] C. Schaschke, *A Dictionary of Chemical Engineering*. OUP Oxford, 2014.

[18] D. G. Owen, T. Schenkel, D. E. T. Shepherd, and D. M. Espino, "Assessment of surface roughness and blood rheology on local coronary haemodynamics: A multi-scale computational fluid dynamics study," *J. R. Soc. Interface*, vol. 17, no. 169, Aug. 2020.